Rhodium-Catalyzed C−C Coupling Reactions: Mechanistic Considerations

Kirsty J. Hawkes,[†,‡] Kingsley J. Cavell,[†,‡] and Brian F. Yates*[,†]

Department of Chemistry, Cardiff University, P.O. Box 912, Cardiff, U.K. CF10 3TB, and School of Chemistry, University of Tasmania, Private Bag 75, Hobart, Tasmania, Australia 7001

Received May 23, 2008

An alternative mechanism for intramolecular C−C coupling between heterocycles and alkenes with rhodium phosphine catalysts is presented involving oxidative addition, alkene insertion, and reductive elimination (route 2), as described previously for similar group 10 reactions by Cavell and McGuinness. Computational studies indicate that the rate-determining step is associated with reductive elimination of the product and overall barriers indicate this mechanism would be competitive with an alternative involving formation of a carbene complex derived from mechanistic work by Bergman, Ellman, and associates (route 1). Activation of the reacting azole through inclusion of an acid catalyst appears to support the route 2 mechanism. A much lower activation barrier is observed under acidic conditions, a result consistent with that found under experimental conditions.

Introduction

Carbon−carbon coupling reactions via transition-metal-catalyzed C−H bond activation have become increasingly important, with applications in many industries, including medicine, energy, and the chemical industry in general.[1−4] An important subset of these reactions includes the C−C coupling of heterocycles, substances abundant in natural product and biological chemistry.[5]

In 2001, Bergman, Ellman, and co-workers reported the very interesting intramolecular coupling of alkenes to heterocycles to create 2-functionalized azoles[6−10] (Figure 1).

In general, the C−C coupling reactions were performed using a $[RhCl(coe)_2]_2$ (coe = cyclooctene) precatalyst in the presence of PCy_3. While the reaction was catalytic at 150 °C with yields frequently in the 70−80% range, addition of a weak acid was found to increase the rate of the reaction considerably.[8]

Variations of the initial reaction included a range of different azoles, incorporating electron-withdrawing and -donating groups in the ring, functionalization built into the reacting alkene, and intermolecular reactions involving free alkenes.[7−10]

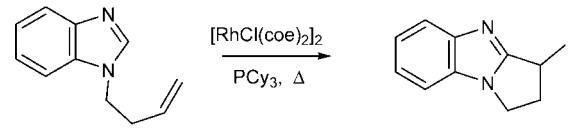

Figure 1. C−C coupling reaction.

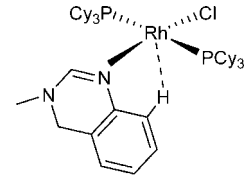

Figure 2. σ-bound rhodium nitrogen complex.

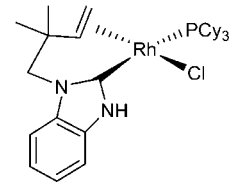

Figure 3. Isolated rhodium carbene intermediate.

As part of their studies, the Bergman−Ellman group included some elegant computational and experimental studies to help elucidate a mechanism for the reaction.

1. Reduction of the reaction temperature below 35 °C resulted in an equilibrium between the free quinazoline/$(PCy_3)_2RhCl$ reactants and a nitrogen-bound quinazoline rhodium complex (Figure 2).[11]

2. Raising the temperature between 45 and 75 °C with the use of stoichiometric quantities of rhodium precatalyst and phosphine ligand led to the isolation of a rhodium(I) carbene

* To whom correspondence should be addressed. E-mail: Brian.Yates@utas.edu.au.

† University of Tasmania.

‡ Cardiff University.

(1) Kakiuchi, F.; Murai, S. In *Activation of Unreactive Bonds in Organic Synthesis*; Murai, S., Ed.; Freund: London, 1999; Vol. 3, pp 47−79.

(2) Ritleng, V.; Sirlin, C.; Pfeffer, M. *Chem. Rev.* **2002**, *102*, 1731–1770.

(3) Guari, Y.; Sabo-Etienne, S.; Chaudret, B. *Eur. J. Inorg. Chem.* **1999**, *104*, 7–1055.

(4) Wiedemann, S. H., Bergman, R. G., Ellman, J. A., Dyker, G., Eds.; Wiley-VCH: Weinheim, Germany, 2005; Vol. 1, pp 187−194.

(5) Schnürch, M.; Flasik, R.; Khan, A. F.; Spina, M.; Mihovilovic, M. D.; Stanetty, P. *Eur. J. Org. Chem.* **2006**, 3283–3307.

(6) Tan, K. L.; Bergman, R. G.; Ellman, J. A. *J. Am. Chem. Soc.* **2001**, *123*, 2685–2686.

(7) Tan, K. L.; Bergman, R. G.; Ellman, J. A. *J. Am. Chem. Soc.* **2002**, *124*, 3202–3203.

(8) Tan, K. L.; Bergman, R. G.; Ellman, J. A. *J. Am. Chem. Soc.* **2002**, *124*, 13964–13965.

(9) Tan, K. L.; Vasudevan, A.; Bergman, R. G.; Ellman, J. A.; Souers, A. J. *Org. Lett.* **2003**, *5*, 2131–2134.

(10) Tan, K. L.; Park, S.; Ellman, J. A.; Bergman, R. G. *J. Org. Chem.* **2004**, *69*, 7329–7335.

(11) Wiedemann, S. H.; Lewis, J. C.; Ellman, J. A.; Bergman, R. G. *J. Am. Chem. Soc.* **2006**, *128*, 2452–2462.

10.1021/om800472v CCC: $40.75
Publication on Web 08/23/2008

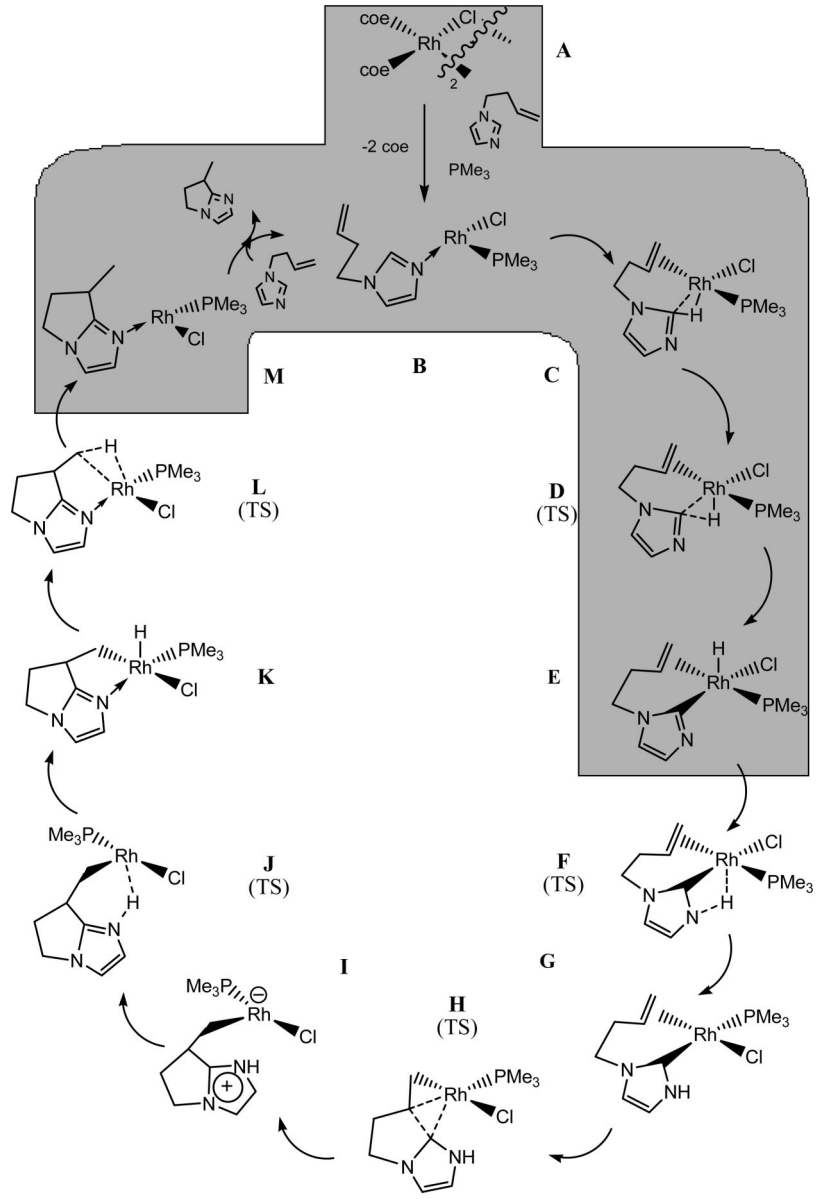

Figure 4. Proposed catalytic cycle for intramolecular C−C coupling of *N*-butenylimidazole: route 1 (TS = transition structure; grayed area indicates intermediates common to the route 2 mechanism (see below)).

complex (Figure 3) which, when reintroduced into a catalytic environment, proceeded with the C−C coupling reaction identical with that established previously.[7]

3. Monitoring the reaction by NMR confirmed that the carbene intermediate was present in significant quantities throughout the reaction sequence, indicating that it is an important intermediate in the catalytic cycle.[7]

4. Deuterium tracers indicated that it is the original azole C2 hydrogen which migrates to the nitrogen to form the carbene complex via a rhodium hydride in an intramolecular reaction.[11]

5. Further deuterium tracers and cross-coupling experiments showed that while there may be rapid alkene insertion into the rhodium−hydride bond and subsequent β-hydride elimination, there was no actual cross-coupling for product formation, indicating that the coupling itself occurs in an intramolecular fashion.[6]

With this information in mind and replacing the PCy_3 ligand with PMe_3, a mechanism based on the combined experimental and theoretical results by Bergman, Ellman, and co-workers[7,11] can be proposed for the C−C coupling from the isolated carbene complex involving insertion of the alkene into the rhodium−carbene bond (Figure 4: **G** → **I**), proton transfer (Figure 4: **I** → **K**) and reductive elimination of the final product (Figure 4: **K** → **B**). It was envisaged that initial C−H activation of the azole via an N-coordinated azole complex (Figure 4: **B** → **E**) to form a rhodium hydride complex followed by hydride migration (Figure 4: **E** → **G**) may be the mechanism by which the carbene complex itself is formed.

The computational study of the initial steps of the reaction for an alkene-free quinazoline[7,11] indicated that the oxidative addition step (**C** → **E**) to create the rhodium hydride presented a modest barrier to reaction, with subsequent formation of the carbene complex (**E** → **G**) being relatively straightforward. Further, the carbene complex **G** proved to be by far the most stable intermediate of all possibilities along the post-carbene pathway,[7,11] a result consistent with the isolation and NMR appearance of the complex under experimental conditions. Overall, the rate-determining step for the post-carbene reaction appeared to be associated with alkene insertion (Figure 4: **G** → **I**).[7,11,72]

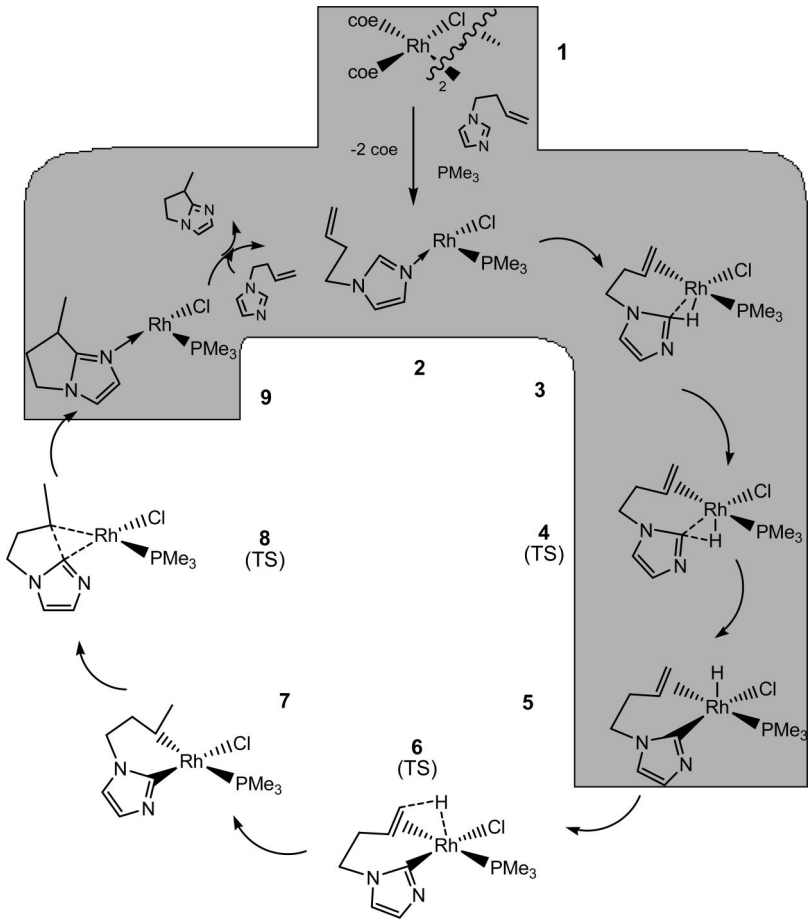

Figure 5. Proposed catalytic cycle for intramolecular C−C coupling of *N*-butenylimidazole: route 2 mechanism (TS = transition structure; grayed area indicates intermediates common to route 1).

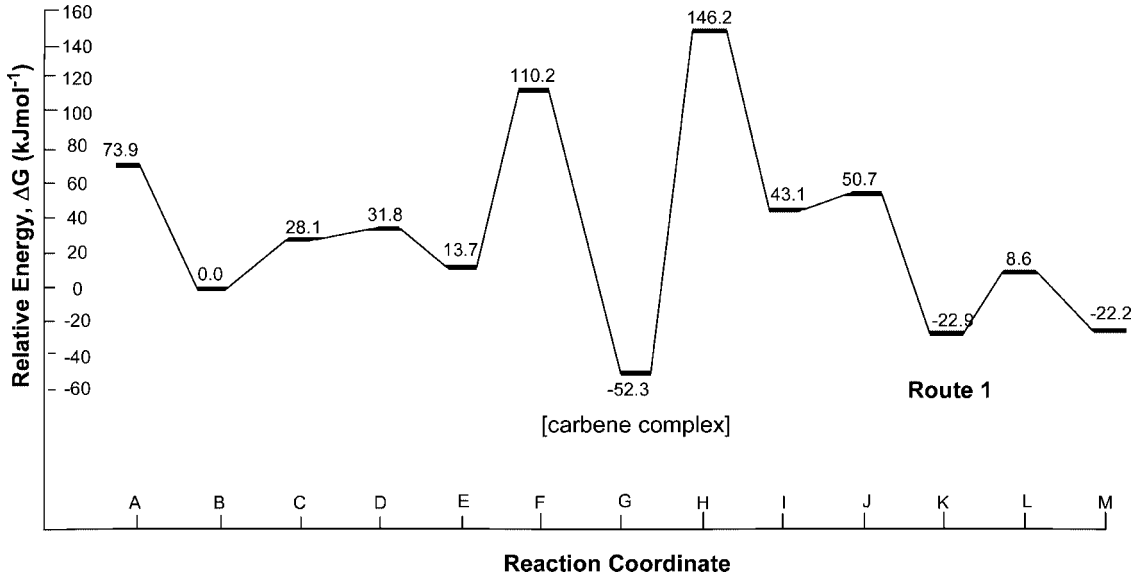

Figure 6. Energies for the route 1 catalytic cycle (reactants: $^1/_2[(coe)_2RhCl]_2$ + PMe_3 + 1-(3-butenyl)imidazole).

Independently, we and others have been interested in the redox behavior of imidazolium salts[12−15] and successful cross-coupling reactions involving nickel[16−20] and palladium[12,13,21−43] carbene catalysts. In particular, we have been investigating a C−C coupling reaction similar to that of Bergman and Ellman's group between alkenes and azolium salts using nickel and palladium phosphine and carbene catalysts.[22,23,44] Experimental and theoretical work on these group 10 transition-metal reactions indicated that the likely mechanism comprises oxidative addition of the azolium salt, alkene coordination, and insertion into the resultant metal hydride, followed by reductive elimination of the coupled product (route 2, Figure 5[73] shown for rhodium and azole equivalent reaction). In general, the rhodium C−C coupling reaction between azoles and alkenes performed by Bergman, Ellman, and co-workers and the azolium salt/alkene coupling studied

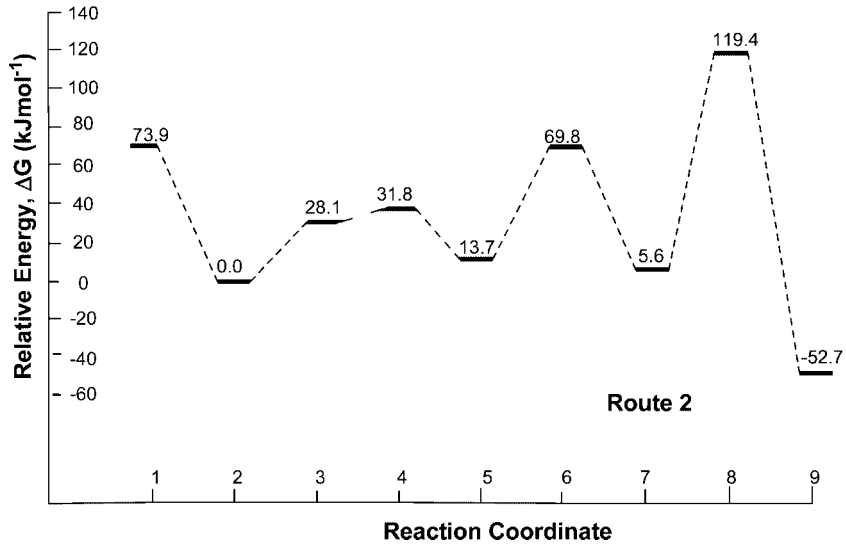

Figure 7. Energies for the route 2 catalytic cycle.

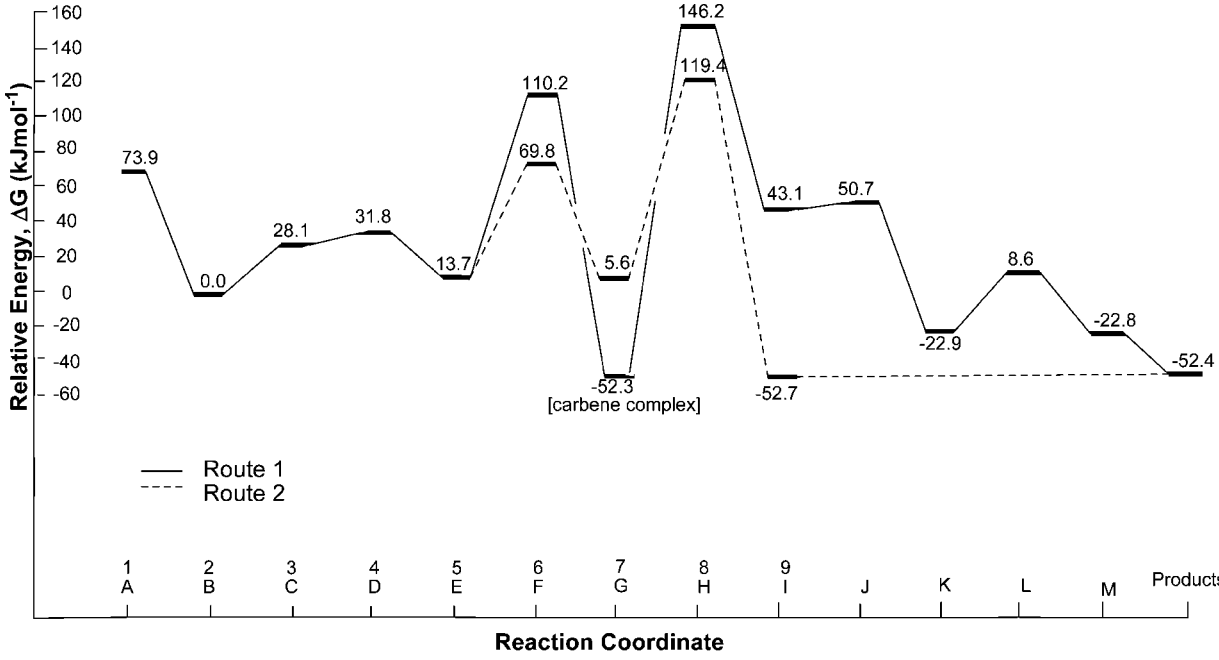

Figure 8. Energy comparison of the route 1 and route 2 mechanisms.

Table 1. Key Free Energies (Dimensionless) and Relative Turnover Frequencies (TOF) for Routes 1 and 2 at 298 K[a,b]

	route 1		route 2 (−carbene complex)		route 2 (+carbene complex)		
	complex	energy	complex	energy	complex	energy	X_{TOF}
MARI[c]	**G**	−21.2	**9**	−21.4	**G**	−21.2	
HETS[d]	**H**	59.4	**8**	48.5	**8**	48.5	0.97
					F	44.8	0.03
$\delta E'$		80.6		48.6[e]		69.7	
relative TOF[f]		1		7.98×10^{13}		5.18×10^{4}	

[a] See ref 66 for detailed methods of calculation. [b] $\Delta G = 21.3$, which refers to the overall process (positive by definition). [c] MARI = most abundant reaction intermediate. [d] HETS = highest energy transition state. [e] $\delta E' = E(\mathbf{8}) - E(\text{MARI}) - \Delta G$, as **8** precedes MARI. [f] TOF values relative to route 1 as standard.

by our group appear quite similar. Further, the proposed mechanism for the rhodium catalysis involved some similar steps, albeit in a modified order and with additional stages. Consequently, we present here a computational study comparing the Bergman, Ellman, and co-workers inspired route 1 (Figure 4) and rhodium-equivalent Cavell−McGuinness inspired route 2 mechanism (Figure 5).

Theoretical Calculations

Geometry optimizations and harmonic vibrational frequencies for all systems were calculated at the B3LYP[45−47] level of theory with the LANL2DZ basis set (which incorporates the Hay and Wadt[48] small-core relativistic effective core potential and double-ζ valence basis set) on rhodium and 6-31G(d) basis set on all other atoms. Zero-point vibrational energy corrections were obtained

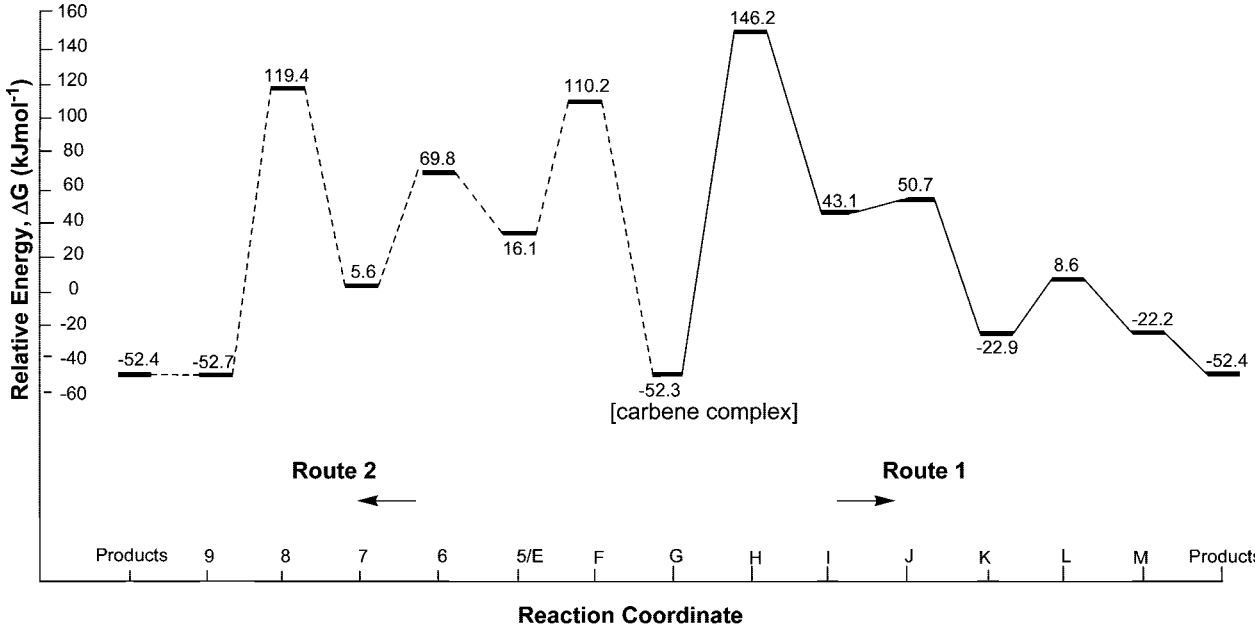

Figure 9. Route 1 and route 2 mechanisms starting from the carbene complex.

Table 2. Rate-Determining Solvation Energies for Route 1 and Route 2

	route 1				route 2		
	F	**G**	**H**	**I**	**7**	**8**	**9**
gas phase	110.2	−52.3	146.2	43.1	5.6	119.4	−52.7
solvation (THF)	123.9	−41.3	140.2	51.5	16.1	130.3	−52.5

Table 3. Key Free Energies (Dimensionless) and Relative TOF Values for Solvated Routes 1 and 2 at 298 K[a,b]

	route 1		route 2		
	complex	energy	complex	energy	X_{TOF}
MARI	**G**	−16.8	**G**	−16.8	
HETS	**H**	56.9	**8**	52.9	0.93
			F	50.3	0.07
$\delta E'$		73.7		69.7	
relative TOF[c]		1		5.09×10^4	

[a] See ref 66 for detailed methods of calculation. [b] $\Delta G = 23.3$, which refers to the overall process (positive by definition). [c] TOF values relative to solvated route 1 as standard.

using unscaled frequencies. All transition structures contained exactly one imaginary frequency and were characterized by following the corresponding normal mode toward the products and reactants.

Higher level single-point calculations were performed on the optimized geometries at the B3LYP level with a LANL2augmented: 6-311+G(2d,p) basis set, incorporating the LANL2 effective core potential and a large LANL2TZ+(3f) basis set on rhodium. This basis set was obtained by us in the same way as described for the Pt LANL2TZ+(3f) basis set reported previously.[49] All other atoms used the 6-311+G(2d,p)[50−52] basis set. Energies from these single-point calculations were combined with the thermodynamic corrections at the lower level of theory to obtain ΔG_{298} numbers. All energies quoted in this paper refer to these final ΔG_{298} values.

Structures **B**, **F**−**I**, and **7**−**9** were reoptimized at the B3LYP level in solvent (THF) with the polarized continuum method of Tomasi and co-workers[53,54] using the integral equation formalism model (IEFPCM)[55−58] with standard tesserae area of 0.2 Å^2, the UAKS parameter set for the united atom topological model for the atomic radii, and the LANL2DZ:6-31G(d) basis set described above. $\Delta G^{solvation}$ was then calculated on the optimized geometries using HF and IEFPCM with the UAHF parameter set for the united atom topological model for the atomic radii with the previously discussed LANL2augmented:6-311+G(2d,p) basis set. The $\Delta G^{solvation}$ values were combined with gas-phase energies to provide the final solvated energies.

All calculations were performed with the Gaussian 03[59] set of programs.

Results and Discussion

Initial Considerations. The mechanistic study by Bergman, Ellman, and co-workers was published over several papers and involved a variety of reacting azoles and phosphine ligands. To allow comparisons between the overall mechanism derived from that work for route 1 and those of our group for route 2, we completed all calculations on each mechanism using model reactants from the experimentally successful catalytic reactions, namely 1-(3-butenyl)imidazole as the reacting azole, $[RhCl(coe)_2]_2$ as the rhodium precursor complex, and 1 equiv of trimethylphosphine (PMe_3).

Use of this particular set of conditions led to a number of considerations in the present study. First, two possible oxidative addition routes were shown previously[7,11] to be competitive in the early stages of the reaction, where the rhodium hydride complex required for carbene formation could be produced either directly from oxidative addition (migration pathway) or indirectly from rotation of the azole ligand once the rhodium hydride had formed (rotation pathway). For simplicity in the energy diagrams we have only included the migration pathway; barriers for each reaction pathway were within 9 kJ mol^{-1} of each other.

Second, the initial study[7,11] of the oxidative addition and carbene formation steps did not involve the presence of an alkene. The competition for oxidative addition over η^2-alkene coordination has been shown previously to be a delicate balance;[60−65] however, as the true catalytic system contained only one phosphine ligand,[15−18] it is expected that the alkene would coordinate to the metal center prior to oxidative addition to alleviate the coordinately unsaturated nature of the rhodium(I) precursor complex.

Finally, crystal structures obtained by Bergman, Ellman, and co-workers for carbene complexes with different azoles resulted in one complex in which the chloride ligand was located trans

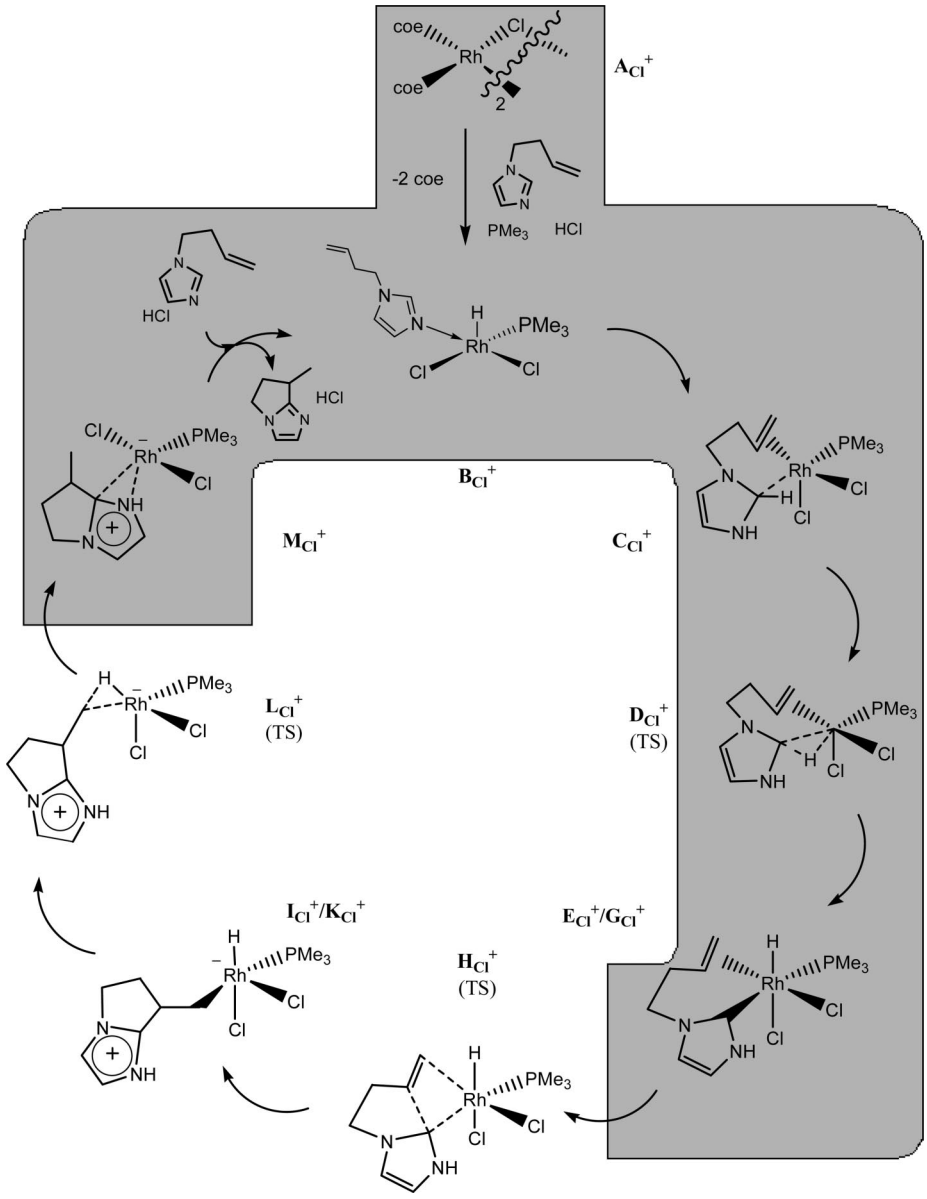

Figure 10. Acid-cocatalyzed route 1 cycle (TS = transition structure; grayed area indicates intermediates common to acid-cocatalyzed route 1 and route 2 mechanisms).

to the carbene ligand,[11] and another in which the chloride was located in the cis position.[7] As these structures formed the basis of the respective computational studies, the oxidative addition and carbene formation results were presented with the trans-located chloride, while the post-carbene mechanism utilized the cis complex. Interestingly, our energy calculations for both cis and trans pathways indicated that the lowest energy pathway for the reaction, prior to carbene formation, is indeed with the chloride ligand trans to the azole ligand, whereas the chloride cis to the carbene is favored in the post-carbene steps.

As it is expected that alkene coordination and cis and trans isomerization would occur relatively easily under experimental conditions, details of these rearrangements are not presented in the main paper, with only the lowest energy configurations shown in the energy diagrams. However the full energy diagrams for all combinations are presented in the Supporting Information.

Complete Route 1 Mechanism. Combining all steps into one cycle results in an interesting overall route 1 mechanism (Figure 6).

First, it should be noted that previous computational results with an *N*-methylazole system indicated that the barrier to oxidative addition (**B** → **E**) was higher than that found for carbene formation (**E** → **G**). While this was also reflected under experimental conditions, the use of the *N*-butenylazole instead of the *N*-methylazole and the presence of only 1 equiv of phosphine inverted the relative energies of these barriers in our calculations. This result is expected with alkene coordination straightforward onto the unsaturated rhodium (**B**) and subsequent chelation drawing the reacting azole close to the metal center. On its own, the initial oxidative addition step is only marginally endothermic with a low activation energy.

Continuing with the catalytic cycle, hydride migration from the oxidative addition product to form the carbene complex (**E** → **G**) requires an additional 96.5 kJ mol^{-1}. While this may not appear restrictive as an individual step, when viewed in sequence, it adds a further barrier to the preliminary steps of the reaction, increasing the overall barrier from the azole N-bound starting complex **B** to the carbene complex to a high 110.2 kJ mol^{-1}.

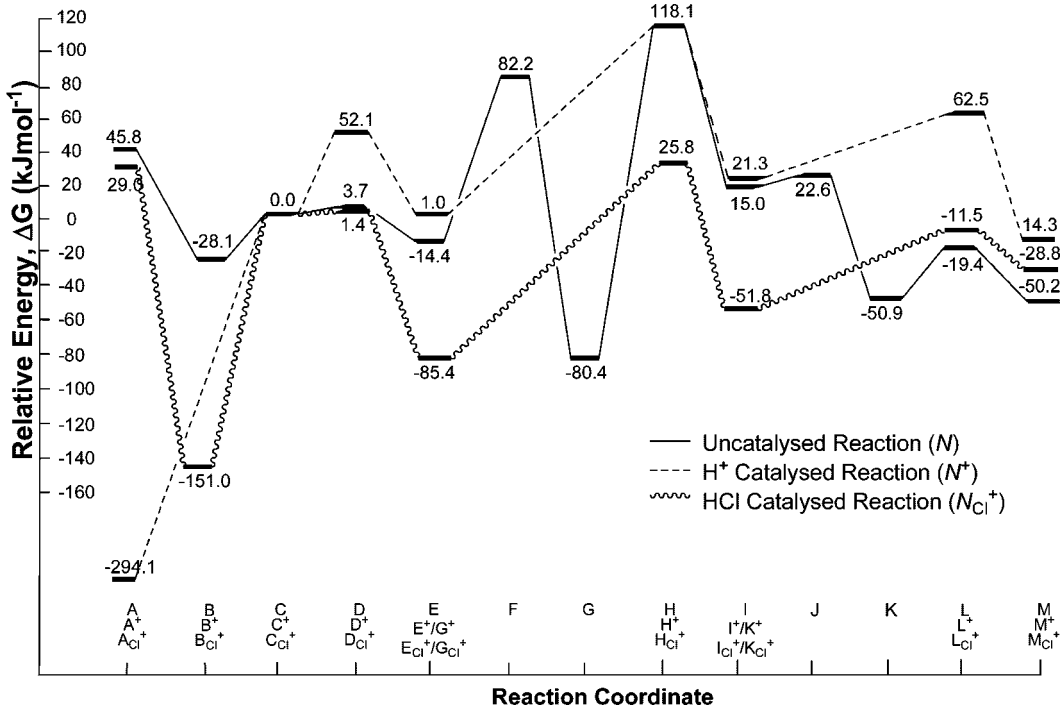

Figure 11. Energies for the acid-cocatalyzed and neutral route 1 cycles.

Despite the challenge of the initial steps of the reaction, formation of the carbene complex results in a remarkably low energy intermediate (**G**). Being 52.3 kJ mol^{-1} lower in energy than the azole N-bound starting complex **B**, this carbene complex is over 29 kJ mol^{-1} more stable than any other of the central intermediates and has high barriers for continued (**G** → **I**) or reverse (**G** → **E**) reaction. Consequently, it is not surprising that Bergman, Ellman, and co-workers were able to isolate this complex under experimental conditions.

Interestingly, continuation of the cycle from the carbene intermediate (**G** → **I**) requires more energy than the reversal of the hydride migration and reductive elimination of the starting materials (**G** → **B**), with activation energies standing at 146.2 and 110.2 kJ mol^{-1}, respectively. This higher barrier is consistent with formation of the carbene complex at temperatures lower than those required for full catalysis. Regardless of whether the reaction proceeds forward or reverts to starting materials, it is expected to be a smooth transition, with all remaining barriers below 33 kJ mol^{-1}.

Complete Route 2 Mechanism. As mentioned previously, the Route 2 mechanism follows a path of oxidative addition (**2** → **5**), alkene insertion (**5** → **7**) and reductive elimination (**7** → **9**). One of the most significant differences between this mechanism and route 1 is the oxidation state of the metal center throughout the catalytic cycle. Route 1 alternates between the formal +1 and +3 charges on the metal for the majority of the catalytic cycle. The intermediates are generally square planar, with only a single phosphine attached to the metal at any one time. In contrast, the route 2 mechanism involves three negatively charged ligands and it is likely that the formal +3 oxidation state remains on the metal for all but the weakly bound reactant and product complexes (**9** → **3**).

Despite this, the initial steps of the route 2 mechanism (**1** → **5**) match those of route 1 (**A** → **E**), with oxidative addition resulting in the formation of the rhodium hydride. From this point, the hydride migration in route 1 is replaced by the coordination and insertion of the alkene into the Rh−H bond (**5** → **7**).

As the geometry optimization of the oxidative addition product indicated that the alkene ligand is the most stable when perpendicular to the Cl−Rh−P plane, only a small movement of the hydride ligand toward the alkene itself is required to reach the insertion transition structure. Consequently, the barrier for the insertion reaction is small at 56.1 kJ mol^{-1} (Figure 7).

While this is very promising for the overall reaction, the resultant alkyl complex **7** is only 8.1 kJ mol^{-1} more stable than the hydride alkene complex **5**. With a moderate barrier to insertion, the reverse β-hydride elimination reaction may occur as rapidly as the formation of the alkyl complex and this step may be seen as a facile yet easily reversible step in the overall reaction; a result reflected in the experimental deuterium tracer results of Bergman, Ellman, and co-workers.[6]

In the final step of the cycle, the reductive elimination energetics combine a reasonable activation barrier with a highly exothermic reaction (**7** → **9**). Standing at 113.8 kJ mol^{-1}, the energy required for reductive elimination is the highest individual barrier along the reaction pathway. Once overcome, however, the energy benefits are considerable with the nitrogen-bound imidazole product **9** reminiscent of that found in the reactants (**2**) and lying 58.3 kJ mol^{-1} lower in energy than the four-coordinate alkyl/acyl complex **7**.

Despite the overall reaction being quite favorable, with the C−C coupled product being 52.7 kJ mol^{-1} lower in energy than the azole N-bound starting complex **B**, it appears that the straight route 2 mechanism studied here would be a challenging one under the reaction conditions. In general, the individual steps have relatively low barriers to reaction; however, an overall activation energy of 119.4 kJ mol^{-1} and no clear lower energy intermediates or catalyst resting states indicate other mechanisms may compete successfully with the route 2 mechanism.

Comparison of the Route 1 and Route 2 Mechanisms. A direct comparison of the energies for the route 1 and route 2 mechanisms reveals some interesting insights into catalytic cycles (Figure 8).

Analysis of these cycles by the method of Kozuch and Shaik[66] indicates that route 2 has a significantly higher turnover

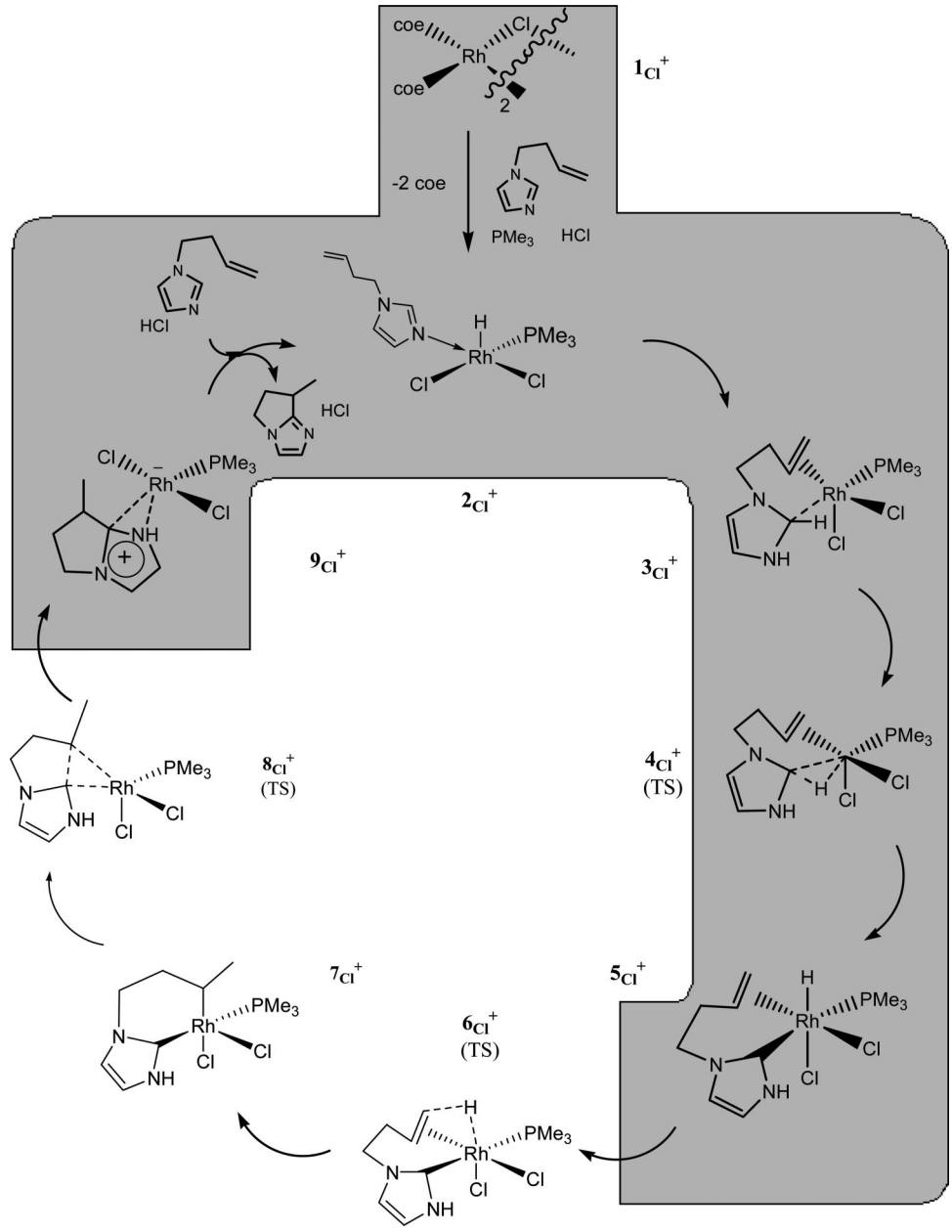

Figure 12. Acid-cocatalyzed route 2 cycle (TS = transition structure; grayed area indicates intermediates common to acid-cocatalyzed route 1 and route 2 mechanisms).

frequency (TOF) under steady-state conditions (Table 1). Both cycles have only one transition structure influencing the TOF: namely, the C−C coupling transition structure (route 1, **G** → **I**; route 2, **7** → **9**). However, the energetic difference ($\delta E'$) between the highest energy transition state (HETS) and the lowest energy intermediate (most abundant reaction intermediate, MARI) is significantly lower for route 2, resulting in a higher TOF (Table 1: route 2 − carbene complex).

While these observations suggest the route 2 mechanism could be active for this reaction, the experimental evidence confirming the presence of the carbene complex by NMR observations during catalysis and the actual isolation of this complex indicate an alternate mechanism may be in operation at certain temperatures. With the exception of the reactants and final products, this complex is by far the most stable intermediate over both routes.

At this point, it is important to observe the barriers on either side of the carbene complex. With these barriers within 36 kJ mol^{-1} of each other, continuation of the cycle in either direction would be feasible. This might suggest that both mechanisms may be operating in tandem, as indicated in Figure 9. It is not unusual for several low-energy pathways to be accessible for a catalytic cycle,[67,68] and interestingly, the isolation and presence of the carbene complex during catalysis with this system is consistent with both mechanisms, as the barrier to carbene formation (**A** → **G**: 110 kJ mol^{-1}) is lower than the barrier to full catalysis by either route (route 1, 146.2 kJ mol^{-1}; route 2, 119.4 kJ mol^{-1}).

Indeed, inclusion of the carbene complex in the overall reaction for route 2 significantly decreases the calculated TOF (Table 1: route 2 + carbene complex). C−C coupling remains the dominant controlling factor in the TOF; however, in this case the barrier associated with formation of the carbene complex also has a minor influence on the overall kinetics. Despite this, results indicate route 2 would remain the preferred route under steady-state conditions.

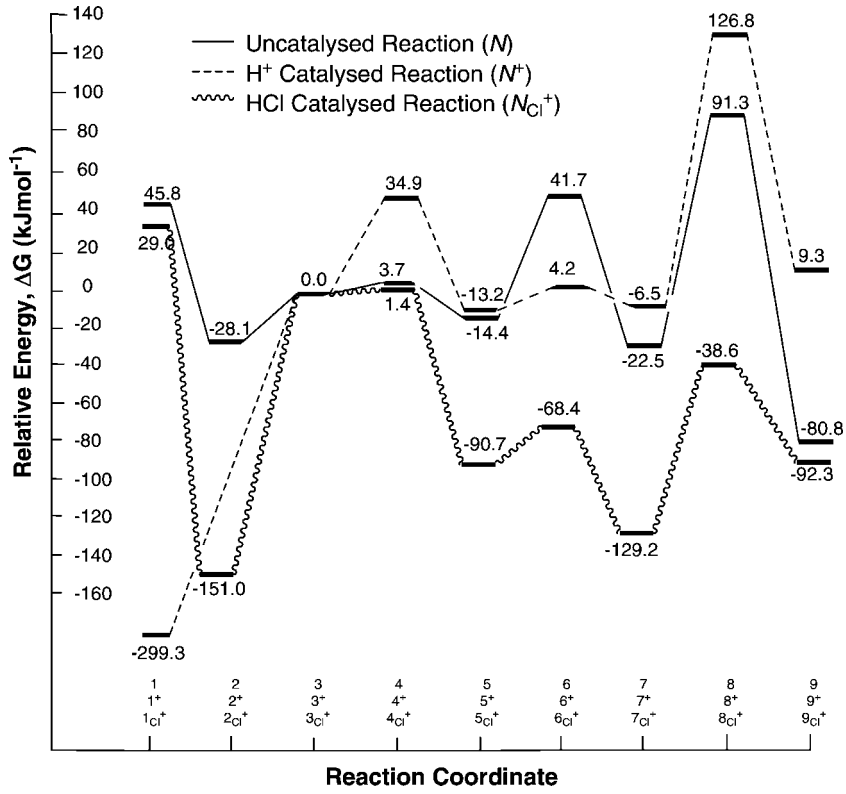

Figure 13. Energies for the acid-cocatalyzed and neutral route 2 cycles.

A further important observation is the nature of some intermediates and their associated transition structures. The rate-determining C−C coupling step of route 1 involves the transformation of the neutral carbene complex **G** into the zwitterionic complex **I**, while route 2 involves straight reductive elimination from rhodium(III) to rhodium(I) (**7** → **9**). With calculations performed in the gas phase, the zwitterionic charge associated with the transition from **G** to **I** is expected to be artificially high, with little charge delocalization possible within the molecule itself. Indeed, solvent reoptimization and energy calculations of the rate-determining complexes for both routes did indicate that the activation energy for route 1 decreases slightly with solvation (Table 2: **G** → **H**), while the activation energy for route 2 remains almost constant (Table 2: **7** → **8**).

Despite these changes in individual activation energies, it should be noted that the TOF for route 2 remains greater than that for route 1 (see Table 3) and, therefore, route 2 most likely remains the more dominant cycle for full catalysis under steady-state conditions.

Interestingly, experimental results to date do not conclusively support or eliminate either mechanism. First, isolation of the carbene complex **G** at lower temperatures and the significant presence of this complex in higher temperature catalytic reactions is consistent with both routes, since in each case (as previously mentioned), the activation barrier to carbene formation (**E** → **G**) is lower than the rate-determining C−C coupling step (route 1, **G** → **I**; route 2, **7** → **9**). While the carbene complex is vital for the route 1 mechanism, it can be thought of as part of a nonessential side reaction for a route 2 mechanism (see Figures 7 and 9); therefore, the absence of this complex should still conceivably result in C−C coupling.

However, two further experimental results indicate this may not be the case. First, use of the bulky PCy_3 ligand in experiments would be expected to decrease the barrier to C−C coupling in comparison to the PMe_3 used in theoretical calculations. Despite this, carbene formation is still prevalent under experimental conditions, indicating the barrier to H migration to form the carbene complex **B** remains below that for C−C coupling. Second, reagents incapable of forming carbene complexes such as pyrimidine and indole have not been successfully coupled, indicating the carbene complex is required for overall catalysis.

Alternatively, deuterium tracer experiments indicate rapid alkene insertion into the M−H bond in solution, followed by β-hydride elimination.[6] This result is strong support for the insertion step for route 2 (**5** → **7**) and, therefore, the presence of **7** under the reaction conditions. With the overall activation barrier for C−C coupling (**7** → **9**) 26.8 kJ mol^{-1} lower than that for route 1 (**G** → **I**), it seems plausible that C−C coupling could occur from the carbene complex via route 2 (Figure 9).

With carbene formation and alkene insertion into the M−H bond both being rapid and facile reactions, the question of which is a "side reaction" and which occurs prior to the rate-determining C−C coupling step is unknown. Further experimental investigation may be possible to help distinguish the two mechanisms in order to further refine and extend these important coupling reactions. In particular, it may be possible to independently verify each step for both mechanisms, as we have done previously for similar nickel-, palladium-, and platinum -based reactions.[14,15,22,23,43]

Acid-Catalyzed Coupling. After successfully catalyzing the cyclization of various alkene heterocycles, Bergman, Ellman, and co-workers made the further observation that the rate and yield of catalysis could be improved by the addition of a weak acid catalyst. In particular, intermolecular coupling was made possible with the use of the Brønsted acid $HClPCy_3$. They proposed a mechanism for the acid-cocatalyzed C−C coupling reaction that involved a carbene complex similar to those described previously (**G**). While not explicitly mentioned, it is assumed the formation of the carbene complex in this acid-

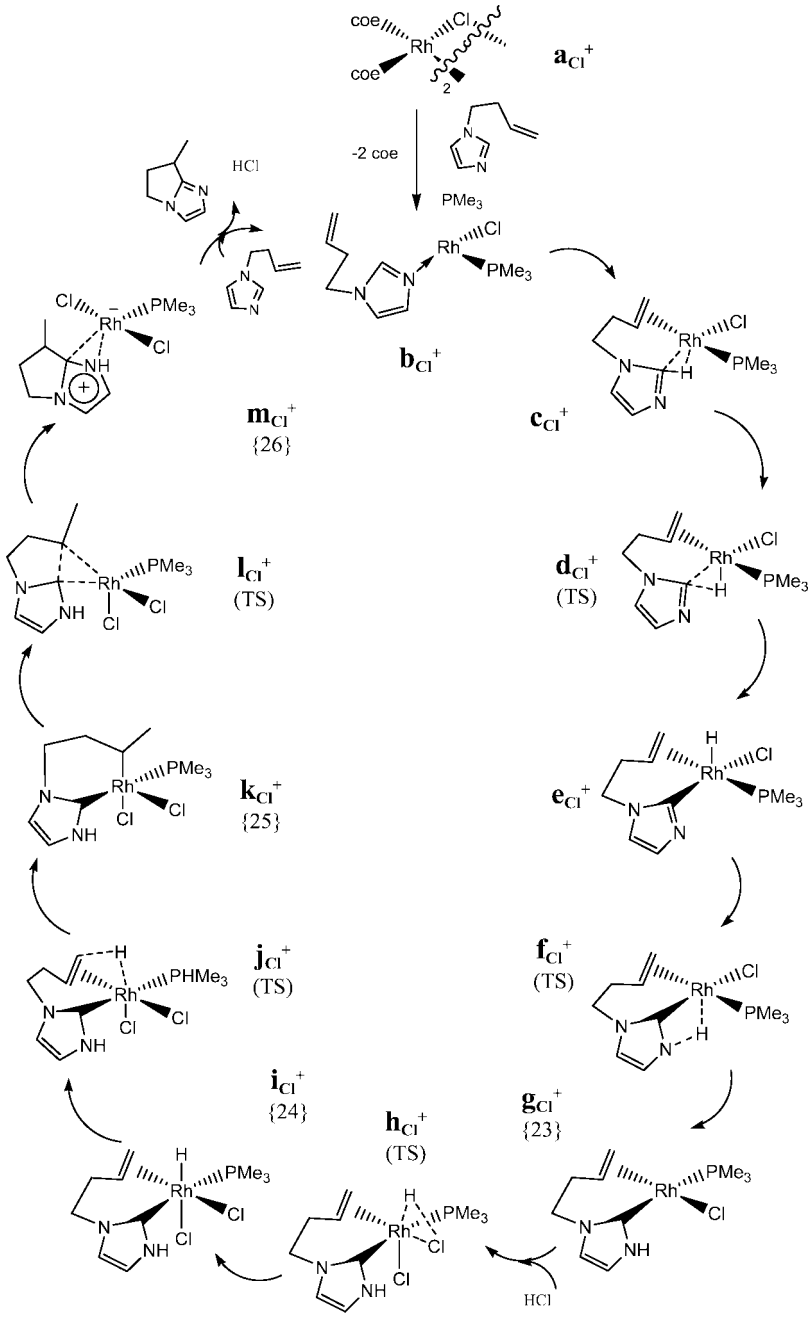

Figure 14. Acid-cocatalyzed route 3 cycle (TS = transition structure, numbers in braces refer to structure labels on mechanism proposed by Bergman, Ellman and co-workers[10]).

cocatalyzed route is via the same mechanism as the noncatalyzed route: i.e., route 1, **A** → **G**. Creation of the carbene complex is followed by oxidative addition of HCl, forming a rhodium(III) hydride to which alkene insertion into the M−H bond results in a rhodium(III) alkyl complex. Alkyl migration creates the coupled product, and the catalytic cycle is regenerated either by reductive elimination of HCl or by addition of a new azole and direct formation of an Rh(III) hydride carbene complex similar to **G**.

With the carbene complex forming under reasonably mild conditions in the absence of an acid cocatalyst, this mechanism seems highly plausible. However, we note that RX addition to an imidazole is a commonly utilized synthesis for the imidazolium salts used as precursors to many transition-metal carbene complexes.[69−71] Further, oxidative addition of such azolium salts has led directly to the formation of transition-metal carbene hydride complexes previously.[22,23] Consequently, we thought it possible that a modified route 1 or route 2 mechanism may exist in the acid-cocatalyzed reaction, in which the catalytic cycle is initiated by oxidative addition of an imidazolium salt in preference to the unactivated imidazole.

As an additional consideration, in the study by Bergman, Ellman, and co-workers the range of successfully coupled reactants was extended and reaction conditions improved exclusively with the use of the coordinating Cl^- anion. Testing of numerous noncoordinating anions provided little benefit and, in some cases, suppressed the reaction altogether. With this clear preference for the coordinating anion in experiment in mind, we undertook a study of the effects of the $HClPMe_3$ additive for the imidazolium salt alternative route 1 and route 2 mechanisms, including both the coordinating and noncoordinating anion instances for comparison. Further, we have included

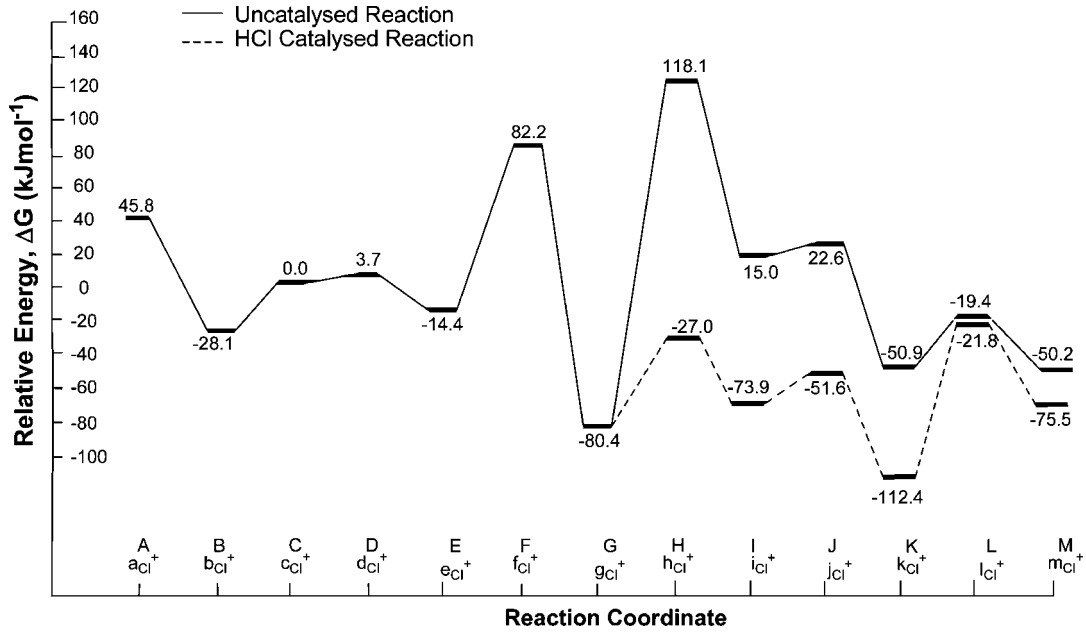

Figure 15. Energies for the route 1 and acid-cocatalyzed route 3 mechanisms.

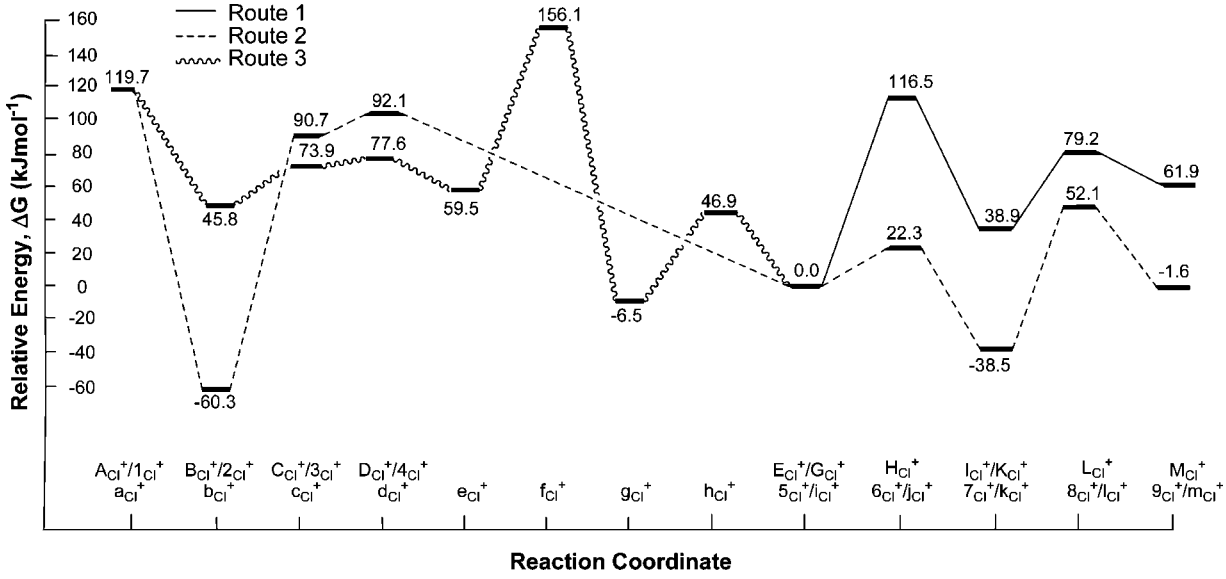

Figure 16. Comparison of acid-catalyzed energies for each of the proposed routes.

Table 4. Key Free Energies (Dimensionless) and Relative TOF Values for Acid-Catalyzed Routes 1−3 at 298 K[a,b]

	route 1		route 2		route 3 (including $\mathbf{B}_{Cl}^+$)	
	complex	energy	complex	energy	complex	energy
MARI	$\mathbf{B}_{Cl}^+$	−24.5	$\mathbf{2}_{Cl}^+$	−24.5	$\mathbf{B}_{Cl}^+$	−24.5
HETS	$\mathbf{H}_{Cl}^+$	47.3	$\mathbf{4}_{Cl}^+$	37.4	$\mathbf{f}_{Cl}^+$	63.4
$\delta E'$	71.8		61.9		87.9	
rel TOF[c]	1		1.99×10^4		1.05×10^{-7}	
rel TOF (uncatalyzed)[d]	6.97×10^3		1.39×10^8		7.32×10^{-4}	

[a] See ref 66 for detailed methods of calculation. [b] $\Delta G = 21.3$, which refers to the overall process (positive by definition). [c] TOF values relative to route 1 as standard. [d] TOF values relative to (uncatalyzed) neutral route 1 as standard.

calculations for the intramolecular adaptation of the catalytic cycle proposed by Bergman, Ellman, and co-workers for the coupling of 1-(3-butenyl)imidazole[18] (route 3) to help elucidate the true catalytic mechanism.

Acid-Catalyzed Route 1 Mechanism. Introduction of an imidazolium salt has a very pronounced effect on the overall reaction sequence for a route 1 acid-cocatalyzed mechanism (Figure 10).[74]

A study of the initial interactions between all reactants indicated that no barrier exists for the oxidative addition of HCl to the $RhCl(PMe_3)$ fragment, with the coordinatively unsaturated $HRhCl_2(PMe_3)$ complex considerably more thermodynamically favored. From here, a particularly stable N-coordinated imidazole complex forms ($\mathbf{B}_{Cl}^+$), reminiscent of the N-bound imidazole complex **B** formed for the neutral catalytic cycle. Protonation of the imidazole nitrogen with subsequent coordina-

tion of the alkene arm forms the oxidative addition precursor $\mathbf{C_{Cl}}^+$. With several low-energy pathways available for formation of the oxidative addition precursor $\mathbf{C_{Cl}}^+$, we have only included the reaction "end points" ($\mathbf{B_{Cl}}^+$ and $\mathbf{C_{Cl}}^+$) in the main paper. Details of the intermediate steps, including a discussion of intra- and intermolecular transfers, are provided in the Supporting Information.

From the oxidative addition precursor complex $\mathbf{C_{Cl}}^+$, the acid-cocatalyzed route 1 mechanism continues in a manner similar to that for the neutral cycle, with a few important changes. Oxidative addition of an imidazolium salt leads directly to a Rh(III) carbene hydride complex ($\mathbf{E_{Cl}}^+/\mathbf{G_{Cl}}^+$), and therefore, the two steps involved in the transformation of **B** to **G** from the neutral route 1 mechanism have been compacted into a single step ($\mathbf{B_{Cl}}^+ \rightarrow \mathbf{E_{Cl}}^+/\mathbf{G_{Cl}}^+$), followed immediately by the insertion of the carbene into the metal−alkene bond ($\mathbf{E_{Cl}}^+/\mathbf{G_{Cl}}^+ \rightarrow \mathbf{I_{Cl}}^+/\mathbf{K_{Cl}}^+$). Reductive elimination of the hydride and alkyl chain creates a C−C-coupled imidazolium salt ($\mathbf{I_{Cl}}^+/\mathbf{K_{Cl}}^+ \rightarrow \mathbf{M_{Cl}}^+$), which transfers a proton back to the metal center ($\mathbf{M_{Cl}}^+ \rightarrow \mathbf{B_{Cl}}^+$). Replacement of the loosely bound salt by an unreacted imidazole resumes the catalytic cycle.

With energies referenced to the oxidative addition precursor complex "**C**" in each case, addition of an acid cocatalyst with a noncoordinating anion provides little benefit for a route 1 mechanism, as reflected under the experimental conditions (Figure 11). Despite a reduction in the number of steps to complete the cycle, the C−C coupling step remains the rate-determining step with a relatively high activation energy of 117.1 kJ mol^{-1} ($\mathbf{E}^+/\mathbf{G}^+ \rightarrow \mathbf{I}^+/\mathbf{K}^+$). Further, no low-energy intermediates are created and oxidative addition and reductive elimination barriers actually increase, indicating an overall deterioration of the likelihood of catalytic reaction.[75]

Inclusion of a coordinating anion into the acid-cocatalyzed cycle provides some interesting results. While it is noted that all intermediates are lower in energy with respect to the oxidative addition precursor $\mathbf{C_{Cl}}^+$, the rate-determining C−C coupling barrier ($\mathbf{E_{Cl}}^+/\mathbf{G_{Cl}}^+ \rightarrow \mathbf{I_{Cl}}^+/\mathbf{K_{Cl}}^+$) is only marginally more favorable than in the noncoordinating anion system at 111.2 kJ mol^{-1}, with other reaction barriers for oxidative addition and reductive elimination remaining constant. As such, it is unlikely a route 1 equivalent mechanism is active under acid-cocatalyzed conditions, as little benefit would be observed experimentally.

Acid-Cocatalyzed Route 2 Mechanism. In contrast to the route 1 acid-cocatalyzed mechanism, introduction of the HCl reactant does not dramatically alter the proposed steps involved in the acid-modified route 2 mechanism (Figure 12). Interestingly, it now becomes clear under acidic conditions that the route 1 and route 2 mechanisms converge to a remarkable degree, with the initial five structures (Figure 10, $\mathbf{A_{Cl}}^+ \rightarrow \mathbf{E_{Cl}}^+/\mathbf{G_{Cl}}^+$; Figure 12, $\mathbf{1_{Cl}}^+ \rightarrow \mathbf{5_{Cl}}^+$) and final structure (Figure 10, $\mathbf{M_{Cl}}^+$; Figure 12, $\mathbf{9_{Cl}}^+$) equivalent in the two cycles.

Despite having little effect on the reaction steps and, indeed, the optimized reaction geometries for the route 2 mechanism, azole N-activation does impact on the energies for the catalytic cycle (Figure 13).

Interestingly, with a noncoordinating anion, the barrier to oxidative addition ($\mathbf{3}^+ \rightarrow \mathbf{5}^+$) is raised compared to that for the neutral reaction. Similarly, while the strength and electron-donating capacity of the carbene ligand helps promote the alkene insertion ($\mathbf{5}^+ \rightarrow \mathbf{7}^+$) reaction, the rate-determining reductive elimination barrier ($\mathbf{7}^+ \rightarrow \mathbf{9}^+$) is raised even further from 113.8 kJ mol^{-1} in the neutral reaction to 133.3 kJ mol^{-1} for a noncoordinating acid cocatalyst. These results indicate, that once again, acid catalysis with a noncoordinating anion would actually be detrimental to the overall reaction.[75]

Despite the failure of a noncoordinating anion system, employment of the coordinating Cl^- anion results in a much more favorable catalytic cycle for a route 2 type mechanism. The activation energy for the rate-determining C−C coupling step (Figure 13, $\mathbf{7_{Cl}}^+ \rightarrow \mathbf{9_{Cl}}^+$) drops to 90.6 kJ mol^{-1}, with the only remaining sizable barrier to reaction being the regeneration of the oxidative addition precursor complex ($\mathbf{9_{Cl}}^+ \rightarrow \mathbf{3_{Cl}}^+$), due mainly to the stability of the azole-coordinated complex $\mathbf{2_{Cl}}^+$. The low energy of all intermediates indicates that the coordinating anion route 2 mechanism appears very plausible.

Acid-Catalyzed Route 3 Mechanism. As mentioned above, Bergman, Ellman, and co-workers proposed an alternative mechanism for the acid-cocatalyzed C−C coupling reaction involving oxidative addition of HCl to the preformed carbene complex. Adaptation of this mechanism for the intramolecular coupling of 1-(3-butenyl)imidazole leads to the catalytic cycle depicted in Figure 14.

With the assumption that the carbene complex forms as proposed for the neutral reaction, this mechanism becomes the combination of the neutral route 1 for formation of the carbene complex (Figure 14, $\mathbf{b_{Cl}}^+ \rightarrow \mathbf{g_{Cl}}^+$), oxidative addition of HCl (Figure 14: $\mathbf{g_{Cl}}^+ \rightarrow \mathbf{i_{Cl}}^+$), with continuation of the cycle (Figure 14, $\mathbf{h_{Cl}}^+ \rightarrow \mathbf{l_{Cl}}^+$) being identical with the final steps in the coordinating route 2 mechanism discussed in the previous section (Figure 12, $\mathbf{5_{Cl}}^+ \rightarrow \mathbf{9_{Cl}}^+$).

(12) McGuinness, D. S.; Cavell, K. J.; Skelton, B. W.; White, A. H. *Organometallics* **1999**, *18*, 1596–1605.
(13) McGuinness, D. S.; Cavell, K. J. *Organometallics* **2000**, *19*, 741–748.
(14) McGuinness, D. S.; Cavell, K. J.; Yates, B. F.; Skelton, B. W.; White, A. H. *J. Am. Chem. Soc.* **2001**, *123*, 8317–8328.
(15) McGuinness, D. S.; Cavell, K. J.; Yates, B. F. *Chem. Commun.* **2001**, *4*, 355–356.
(16) Böhm, V. P. W.; Weskamp, T.; Gstöttmayr, C. W. K.; Herrmann, W. A. *Angew. Chem., Int. Ed.* **2000**, *39*, 1602–1604.
(17) Böhm, V. P. W.; Gstöttmayr, C. W. K.; Weskamp, T.; Herrmann, W. A. *Angew. Chem., Int. Ed.* **2001**, *40*, 3387–3389.
(18) Blakey, S. B.; MacMillan, D. W. C. *J. Am. Chem. Soc.* **2003**, *125*, 6046–6047.
(19) Omar-Amrani, R.; Thomas, A.; Brenner, E.; Schneider, R.; Fort, Y. *Org. Lett.* **2003**, *5*, 2311–2314.
(20) Kuhl, S.; Fort, Y.; Schneider, R. *J. Organomet. Chem.* **2005**, *690*, 6169–6177.
(21) Clement, N. D.; Cavell, K. J. *Angew. Chem., Int. Ed.* **2004**, *43*, 3845–3847.
(22) Clement, N. D.; Cavell, K. J.; Jones, C.; Elsevier, C. J. *Angew. Chem., Int. Ed.* **2004**, *43*, 1277–1279.
(23) Clement, N. D.; Cavell, K. J. *Angew. Chem., Int. Ed.* **2004**, *43*, 3845–3847.
(24) Herrmann, W. A.; Elison, M.; Fischer, M.; Köcher, C.; Artus, G. R. J. *Angew. Chem., Int. Ed.* **1995**, *34*, 2371–2374.
(25) Herrmann, W. A.; Reisinger, C. P.; Spiegler, M. *J. Organomet. Chem.* **1998**, *557*, 93–96.
(26) Stauffer, S. R.; Lee, S.; Stambuli, J. P.; Hauck, S. I.; Hartwig, J. F. *Org. Lett.* **2000**, *2*, 1423–1426.
(27) Herrmann, W. A.; Böhm, V. P. W.; Gstöttmayr, C. W. K.; Grosche, M.; Reisinger, C. P.; Weskamp, T. *J. Organomet. Chem.* **2001**, *617−618*, 616–628.
(28) Loch, J. A.; Albrecht, M.; Peris, E.; Mata, J.; Faller, J. W.; Crabtree, R. H. *J. Organomet. Chem.* **2002**, *653*, 69–82.
(29) Andrus, M. B.; Song, C.; Zhang, J. *Org. Lett.* **2002**, *4*, 2079–2082.
(30) Arentsen, K.; Caddick, S.; Cloke, F. G. N.; Herrin, A. P.; Hitchcock, P. B. *Tetrahedron Lett.* **2004**, *45*, 3511–3515.
(31) Hadei, N.; Kantcher, E. A. B.; O'Brien, C. J.; Organ, M. G. *J. Org. Chem.* **2005**, *70*, 8503–8507.
(32) Gstöttmayr, C. W. K.; Böhm, V. P. W.; Herdtweck, E.; Grosche, M.; Herrmann, W. A. *Angew. Chem., Int. Ed.* **2002**, *41*, 1363–1365.
(33) Altenhoff, G.; Goddard, R.; Lehmann, C. W.; Glorius, F. *Angew. Chem., Int. Ed.* **2003**, *42*, 3690–3693.
(34) Selvakumar, K.; Zapf, A.; Beller, M. *Org. Lett.* **2002**, *4*, 3031–3033.

As indicated in Figure 15, oxidative addition of HCl to the carbene complex ($\mathbf{g_{Cl}}^+ \rightarrow \mathbf{i_{Cl}}^+$) decreases the relative energy for all remaining intermediates of the catalytic cycle in comparison to those for the neutral route ($\mathbf{G} \rightarrow \mathbf{I}$). In particular, the activation energy for the C−C coupling step reduces dramatically from 198.5 kJ mol^{-1} for the noncatalyzed route ($\mathbf{G} \rightarrow \mathbf{I}$) to 90.6 kJ mol^{-1} for the HCl-catalyzed route ($\mathbf{k_{Cl}}^+ \rightarrow \mathbf{m_{Cl}}^+$).

With such low barriers to reaction, it appears creation of the carbene complex itself would become the rate-determining step if route 3 were operative under acidic conditions. This result is particularly interesting in light of experimental results, in which the carbene complex forms under very mild conditions without the aid of an acid cocatalyst.

Overall Acid Catalysis Effects. Energy calculations for all three mechanisms generally reflect the results found under experimental conditions, with the acid-cocatalyzed reaction only enhancing the reaction when a coordinating anion is employed. To further elucidate which of the three mechanisms is preferred under experimental conditions, a direct comparison for the three coordinating anion systems is made possible with the observation that each route proceeds through an identical hydride intermediate (route 1, $\mathbf{E_{Cl}}^+/\mathbf{G_{Cl}}^+$; route 2, $\mathbf{5_{Cl}}^+$; route 3, $\mathbf{i_{Cl}}^+$).

A comparison of the energies for all three acid-cocatalyzed mechanisms referenced to this intermediate reveals some interesting information (Figure 16).

As mentioned in the previous section, the initial steps of the acid-cocatalyzed reaction with a coordinating anion are shared by routes 1 and 2 (Figure 16, $\mathbf{A_{Cl}}^+ \rightarrow \mathbf{E_{Cl}}^+/\mathbf{G_{Cl}}^+$ and $\mathbf{1_{Cl}}^+ \rightarrow \mathbf{5_{Cl}}^+$, respectively). Similarly, the final insertion and reductive elimination steps are shared by routes 2 and 3 (Figure 16, $\mathbf{5_{Cl}}^+ \rightarrow \mathbf{9_{Cl}}^+$ and $\mathbf{i_{Cl}}^+ \rightarrow \mathbf{m_{Cl}}^+$). Further, the difference between the route 1 and route 2 mechanisms becomes one of timing. Both follow a path of oxidative addition, insertion, and reductive elimination; however, in the route 2 case the insertion is the alkene into the metal−hydride bond ($\mathbf{5_{Cl}}^+ \rightarrow \mathbf{7_{Cl}}^+$), while the route 1 mechanism requires insertion of the carbene into the metal−alkene bond ($\mathbf{E_{Cl}}^+/\mathbf{G_{Cl}}^+ \rightarrow \mathbf{I_{Cl}}^+/\mathbf{K_{Cl}}^+$). In addition, the reductive elimination steps involve C−C reductive elimination (route 2 mechanism: $\mathbf{7_{Cl}}^+ \rightarrow \mathbf{9_{Cl}}^+$) compared to C−H reductive elimination (route 1 mechanism: $\mathbf{I_{Cl}}^+/\mathbf{K_{Cl}}^+ \rightarrow \mathbf{M_{Cl}}^+$). As such, it is unsurprising route 2 has a lower barrier to insertion and, conversely, route 1 has a lower barrier to reductive elimination.

Once again, within the actual catalytic cycle the C−C coupling step remains the highest individual barrier for all three mechanisms, regardless of the exact mechanism (note: $\mathbf{B_{Cl}}^+/\mathbf{2_{Cl}}^+$ to $\mathbf{C_{Cl}}^+/\mathbf{3_{Cl}}^+$ is a actually a multistep process with low-energy intermediates, as outlined in the Supporting Information). Despite this, the route 2 and route 3 mechanism barrier is considerably lower at 90.6 kJ mol^{-1} ($\mathbf{7_{Cl}}^+ \rightarrow \mathbf{9_{Cl}}^+$ and $\mathbf{k_{Cl}}^+ \rightarrow \mathbf{m_{Cl}}^+$) compared to 116.5 kJ mol^{-1} for route 1 ($\mathbf{E_{Cl}}^+/\mathbf{G_{Cl}}^+ \rightarrow \mathbf{I_{Cl}}^+/\mathbf{K_{Cl}}^+$).

(35) Selvakumar, K.; Zapf, A.; Spannenberg, A.; Beller, M. *Chem. Eur. J.* **2002**, *8*, 3901–3906.
(36) Frisch, A. C.; Rataboul, F.; Zapf, A.; Beller, M. *J. Organomet. Chem.* **2003**, *687*, 403–409.
(37) Viciu, M. S.; Germaneau, R. F.; Navarro, O.; Stevens, E. D.; Nolan, S. P. *Organometallics* **2002**, *21*, 5470–5472.
(38) Viciu, M. S.; Kelly, R. A.; Stevens, E. D.; Naud, F.; Studer, M.; Nolan, S. P. *Org. Lett.* **2003**, *5*, 1479–1482.
(39) Navarro, O.; Kelly, R. A.; Nolan, S. P. *J. Am. Chem. Soc.* **2003**, *125*, 16194–16195.
(40) Navarro, O.; Oonishi, Y.; Kelly, R. A.; Stevens, E. D.; Briel, O.; Nolan, S. P. *J. Organomet. Chem.* **2004**, *689*, 3722–3727.
(41) Navarro, O.; Marion, N.; Oonishi, Y.; Kelly, R. A.; Nolan, S. P. *J. Org. Chem.* **2006**, *71*, 685–692.
(42) Marion, N.; Navarro, O.; Mei, J.; Stevens, E. D.; Nolan, S. P. *J. Am. Chem. Soc.* **2006**, *128*, 4101–4111.
(43) Clement, N. D.; Cavell, K. J.; Ooi, L. *Organometallics* **2006**, *25*, 4155–4165.
(44) Bacciu, D.; Cavell, K. J.; Fallis, I. A.; Ooi, L. *Angew. Chem., Int. Ed.* **2005**, *44*, 5282–5284.
(45) Hertwig, R. H.; Koch, W. *Chem. Phys. Lett.* **1997**, *268*, 345–351.
(46) Stephens, P. J.; Devlin, J. F.; Chabalowski, C. F.; Frisch, M. J. *J. Phys. Chem.* **1994**, *98*, 11623–11627.
(47) Becke, A. D. *J. Chem. Phys.* **1993**, *98*, 5648–5652.
(48) Hay, P. J.; Wadt, W. R. *J. Chem. Phys.* **1985**, *82*, 299–310.
(49) Yates, B. F. *J. Mol. Struct. (THEOCHEM)* **2000**, *506*, 223–232.
(50) Frisch, M. J.; Pople, J. A.; Binkley, J. S. *J. Chem. Phys.* **1984**, *80*, 3265–3269.
(51) McLean, A. D.; Chandler, G. S. *J. Chem. Phys.* **1980**, *72*, 5639–5648.
(52) Krishnan, R.; Binkley, J. S.; Seeger, R.; Pople, J. A. *J. Chem. Phys.* **1980**, *72*, 650–654.
(53) Barone, V.; Cossi, M. *J. Phys. Chem.* **1998**, *102*, 1995–2001.
(54) Miertus, S.; Tomasi, J. *Chem. Phys.* **1982**, *65*, 239–245.
(55) Mennucci, B.; Cancès, E.; Tomasi, J. *J. Phys. Chem. B* **1997**, *101*, 10506–10517.
(56) Mennucci, B.; Tomasi, J. *J. Chem. Phys.* **1997**, *106*, 5151–5158.
(57) Cancès, E.; Mennucci, B.; Tomasi, J. *J. Chem. Phys.* **1997**, *107*, 3032–3041.
(58) Tomasi, J.; Mennucci, B.; Cancès, E. *J. Mol. Struct. (THEOCHEM)* **1999**, *464*, 211–226.
(59) Frisch, M. J. ; Trucks, G. W.; Schlegel, H. B.; Scuseria, G. E.; Robb, M. A.; Cheeseman, J. R.; Montgomery Jr., J. A.; Vreven, T.; Kudin, K. N.; Burant, J. C.; Millam, J. M.; Iyengar, S. S.; Tomasi, J.; Barone, V.; Mennucci, B.; Cossi, M.; Scalmani, G.; Rega, N.; Petersson, G. A.; Nakatsuji, H.; Hada, M.; Ehara, M.; Toyota, K.; Fukuda, R.; Hasegawa, J.; Ishida, M.; Nakajima, T.; Honda, Y.; Kitao, O.; Nakai, H.; Klene, M.; Li, X.; Knox, J. E.; Hratchian, H. P.; Cross, J. B.; Adamo, C.; Jaramillo, J.; Gomperts, R.; Stratmann, R. E.; Yazyev, O.; Austin, A. J.; Cammi, R.; Pomelli, C.; Ochterski, J. W.; Ayala, P. Y.; Morokuma, K.; Voth, G. A.; Salvador, P.; Dannenberg, J. J.; Zakrzewski, V. G.; Dapprich, S.; Daniels, A. D.; Strain, M. C.; Farkas, O.; Malick, D. K.; Rabuck, A. D.; Raghavachari, K.; Foresman, J. B.; Ortiz, J. V.; Cui, Q.; Baboul, A. G.; Clifford, S.; Cioslowski, J.; Stefanov, B. B.; Liu, G.; Liashenko, A.; Piskorz, P.; Komaromi, I.; Martin, R. L.; Fox, D. J.; Keith, T.; Al.Laham, M. A.; Peng, C. Y.; Nanayakkara, A.; Challacombe, M.; Gill, P. M. W.; Johnson, B.; Chen, W.; Wong, M. W.; Gonzalez, C.; Pople, J. A. Gaussian03, Revision C.02 ed.; Gaussian, Inc., Wallingford, CT, 2004.
(60) Slagt, M. Q.; van Zwieten, D. A. P.; Moerkerk, A. J. C. M.; Gebbink, R. J. M. L.; van Koten, G. *Coord. Chem. Rev.* **2004**, *248*, 2275–2282.
(61) Zapf, A.; Beller, M. *Chem. Commun.* **2005**, *4*, 431–440.
(62) Espinet, P.; Echavarren, M. *Angew. Chem., Int. Ed.* **2004**, *43*, 4704–4734.
(63) van der Boom, M. E.; Milstein, D. *Chem. Rev.* **2003**, *103*, 1759–1792.
(64) Elsevier, C. J. *Coord. Chem. Rev.* **1999**, *185−186*, 809–822.
(65) Lucassen, A. C. B.; Shimon, L. J. W.; van der Boom, M. E. *Organometallics* **2006**, *25*, 3308–3310.
(66) Kozuch, S.; Shaik, S. *J. Am. Chem. Soc.* **2006**, *128*, 3355–3365.
(67) Braga, A. A. C.; Ujaque, G.; Maseras, F. *Organometallics* **2006**, *25*, 3647–3658.
(68) Goossen, L. J.; Koley, D.; Hermann, H.; Thiel, W. *Organometallics* **2006**, *25*, 54–67.
(69) Herrmann, W. A. *Angew. Chem., Int. Ed.* **2002**, *41*, 1290–1309.
(70) Weskamp, T.; Böhm, V. P. W.; Herrmann, W. A. *J. Organomet. Chem.* **2000**, *600*, 12–22.
(71) Bourissou, D.; Guerret, O.; Gabbaï, F.; Bertrand, G. *Chem. Rev.* **2000**, *100*, 39–91.
(72) While different azole and phosphines were used in the two computational studies by the Bergman−Ellman group, a preliminary comparison by us on the overall mechanism indicated the rate-determining step remains unaltered with minor modifications to the azole and phosphine ligands.
(73) **M** and **9** are slightly different in following transition structures **L** and **8**, respectively; however, they are related by minor conformational twists which would be negligible under experimental conditions.
(74) One Cl^- ligand is removed from each structure for the acid-cocatalyzed mechanisms with a noncoordinating anion, $C^+ \rightarrow M^+$.
(75) As a further note, the barriers to reach the oxidative addition precursors $\mathbf{C}^+$ and $\mathbf{3}^+$ are found to be a high 294.1 and 299.3 kJ mol^{-1}, respectively. However, this is an artificially high barrier, due to the presence of the Cl^- ion under gas-phase calculations, and use of a true noncoordinating anion under experimental conditions would considerably reduce this initial barrier.

From a catalysis point of view, the overall reaction is an interesting one, with the standout feature being the stability of the N-bound azole starting complex $\mathbf{B_{Cl}}^+/\mathbf{2_{Cl}}^+$. While it is not directly involved in the route 3 catalytic cycle, the ease of formation and relative low energy of this complex would indicate its involvement in any reaction mixture, therefore becoming the "starting" complex of all three routes and the most abundant reaction intermediate under steady-state conditions. With this in mind, the results strongly indicate a favoring of the route 2 mechanism for the acid-cocatalyzed reaction (Table 4). In contrast to the acid-free reaction, oxidative addition becomes the TOF controlling transition structure for route 2 and a significantly higher TOF is found relative to those for the equivalent route 1 and 3 mechanisms.

Another interesting feature highlighted in Table 4 is the benefit (as seen experimentally) from employing an acid cocatalyst. On comparison directly with the non-acid-cocatalyzed reactions in Table 1 there is a large increase in the overall TOF for routes 1 and 2. In particular, the TOF for the favored route 2 increases by a factor of 10^3. Overall, these results indicate catalysis with an acid cocatalyst containing a coordinating anion would enhance the C−C coupling reaction, as found experimentally, and would most likely proceed via a mechanism represented by route 2.

Conclusions

Two neutral mechanisms for intramolecular coupling have been investigated in this paper. Overall, it is not clear-cut whether the route 1 (C−H oxidative addition, hydride migration, alkenyl M-C insertion, C−H reductive elimination) or route 2 (C−H oxidative addition, alkenyl M-H insertion, C−C reductive elimination) mechanism would be preferred under experimental conditions. Insertion of the carbene into the alkene-metal bond in route 1 appears restrictive with an activation barrier of 198.5 kJ mol^{-1}, while the rate determining reductive elimination of the C−C coupled azole in the route 2 mechanism has a comparatively smaller barrier of 113.8 kJ mol^{-1}. However, as indicated in Figure 9, if catalysis were initiated from the carbene complex isolated by Bergman, Ellman and co-workers, either route may be followed depending on whether carbene insertion or hydride migration occurs first. Despite this, calculations of TOF indicate route 2 would be the favored mechanism under steady-state conditions.

Additional experimental work is required to elucidate the true mechanism or, indeed, confirm the applicability of both mechanisms. Despite this, it appears that the overall neutral catalytic process would benefit from optimization of the C−C coupling step itself or destabilization of the carbene complex, regardless of which mechanism is followed.

Further experimental results by Bergman, Ellman, and coworkers indicate that inclusion of a Brønsted acid increases the rate of the reaction significantly. Interestingly, noncoordinating counterions were found to be detrimental to the reaction, and theoretical results presented here confirm this finding, with overall barriers being reduced considerably only when the coordinating Cl^- counterion is employed. Despite there being no obviously favored mechanism for the neutral azole C−C coupling reaction (i.e., without a Brønsted acid present), it appears that the route 2 mechanism will be followed if an acid catalyst is included in the reaction mixture. While all three acid-cocatalyzed routes studied share an identical intermediate, activation of the imidazole nitrogen to create an azolium-like salt favors the sequence of reaction steps in the route 2 mechanism with the introduction of a very low energy starting complex. In contrast to the neutral reaction, optimization of the acid-catalyzed oxidative addition step would help reduce overall reaction barriers further and assist in the advancement and extension of this important C−C coupling reaction.

Acknowledgment. We wish to thank the Australian and Tasmanian Partnerships for Advanced Computing (APAC and TPAC) for supercomputing time and the Australian Research Council for funding and Professors Bergman and Ellman and their groups for helpful discussions.

Supporting Information Available: Tables giving pictures, energies, and Cartesian coordinates (*XYZ*) for complete route 1, route 2, acid-catalyzed route 1, acid-catalyzed route 2, and acid-catalyzed route 3 mechanisms including cis/trans isomerization. This material is available free of charge via the Internet at http://pubs.acs.org.

OM800472V